Modeling and Analysis of MHD Free Convective Thermo-Solutal Transport in Casson Fluid Flow with Radiative Heat Flux

C. Sowmiya[1], B. Rushi Kumar[1*], O. Anwar Bég[2], Sireetorn Kuharat[2]

[1*]Department of Mathematics, School of Advanced Sciences, Vellore Institute of Technology, Vellore, 632 014, Tamil Nadu, India.
[2]Multi-Physical Engineering Sciences Group, Mechanical Engineering, Salford University, UK.

Abstract

This research paper presents a novel mathematical model aimed at exploring practical applications in oscillating MHD generators and near-wall flows using Casson fluid. The purpose of this study is to develop a mathematical model that specifically addresses MHD free convective thermo-solutal transport within Casson fluid flow over a rotating vertical wall into a permeable medium. This research also considers factors like the Soret effect, radiative heat flux, first-order chemical reactions, and heat source/sink effects. To tackle this complex scenario, we apply the Laplace transform technique (LTT) to handle the transformed partial differential equations and their accompanying boundary conditions. The study investigated both ramped and isothermal wall temperature conditions and evaluated the influence of various parameters, including the Soret number, Hall current parameter, ramped wall temperature, and magnetic body force parameter. The computational analysis is carried out using MATLAB software. The research involves a comprehensive parametric analysis that thoroughly examines the impact of key emerging parameters on generalized velocity, temperature, and species concentration. The results reveal that magnetic, Casson, and rotating parameters all have a diminishing impact on the velocity profiles. The radiation parameter has a positive impact on temperature distribution, while an opposite trend is observed for the Prandtl number. Furthermore, an increase in the Soret number and chemical reaction parameter leads to a decrease in species concentration and solutal boundary layer thickness. The validation process includes comparisons with previous studies. Additionally, this study presents distributions of skin friction, Nusselt number, and Sherwood number. Notably, our findings reveal that a ramped wall temperature results in lower velocity magnitudes compared to the isothermal wall case.

Keywords: MHD generators, Oscillating flows, Hall current, Casson fluid flow, Soret effect, Laplace Transform approach,

1 Introduction

In fluid dynamics and heat transfer studies, the choice of boundary conditions significantly influences the behavior and characteristics of the flow and temperature distribution within a system. Two commonly encountered boundary conditions in thermal analysis are ramped wall temperature and isothermal temperature. These boundary conditions play a crucial role in various engineering and scientific applications, affecting processes such as heat transfer, fluid flow, and thermal stability. Ramped wall temperature refers to a boundary condition where the temperature at the wall changes gradually over time. This gradual temperature change can arise due to external factors such as heating or cooling mechanisms, or as a result of internal processes within the system. Ramped wall temperature conditions are prevalent in scenarios where the system undergoes transient thermal behavior, such as during startup or shutdown processes, or when subjected to time-varying thermal inputs. Sethy et al.[1] analyzed the behavior of Casson hybrid nanofluids in various flow configurations, Mohanty et al.[2] considered factors such as permeability, Debashis et al. [3] investigated interfacial nanolayer thickness, slip velocities, and thermal effects like Joule heating and nonlinear radiation. The analyses aim to understand thermal control, irreversibility, and flow characteristics in complex fluid dynamics scenarios.

Casson fluid is a non-Newtonian fluid model that describes the rheological behavior of certain fluids, particularly those with yield stress. It was named after the British rheologist Ralph A. H. Casson, who introduced the model in 1950. Unlike Newtonian fluids, which exhibit linear stress-strain behavior, Casson fluids exhibit a nonlinear relationship between shear stress and shear rate. The Casson fluid model is characterized by two parameters: the yield stress (τ_0) and the Casson viscosity (μ_C).

The yield stress represents the minimum stress required to initiate flow, while the Casson viscosity denotes the apparent viscosity of the fluid at low shear rates. Ali et al. [4] examined the yield stress, Casson fluid behaves as a solid, exhibiting no flow. [5] analysed the yield stress, the fluid undergoes shear thinning behavior, with viscosity decreasing as the shear rate increases. Oyelakini et al. [6] investigated thermal and irreversibility aspects of unsteady hybrid nanofluid flow over a spinning sphere with Cattaneo-Christov heat flux and interfacial nanolayer mechanism. Additionally, Mohanty et al. [7] analyzed the irreversibility of unsteady micropolar CNT-blood nanofluid flow through a squeezing channel, with implications for drug delivery, Naresh et al. [8] elucidated fluid dynamics and thermal behaviors in nanofluidic systems. [9, 10] analysed interparticle spacing and nanoparticle radius on the radiative alumina-based nanofluid flow subject to irregular heat source/sink over a spinning disk. [11–13] examined thermal convection in rotating ferromagnetic liquid, incorporating thermorheological and magnetorheological effects. It also investigates the impacts of nanoparticle aggregation and thermophoretic particle deposition on nanofluid flow over a Riga wedge, offering mathematical insights into complex fluid dynamics phenomena. Ali et al. [14] examined the mixed convective flow of hybrid nanofluid over a heated stretching disk with zero-mass flux using the modified Buongiorno model.

The analysis of magnetohydrodynamic (MHD) viscous flows holds significant importance in modern industrial systems Muller and Buhler[15], involving the interaction of magnetic fields with electrically conducting fluids Sivaraj[16]. This has led to various applications Ho[17], such as hydromagnetic pumps in nuclear engineering Homsy et al.[18], actuation systems in magneto-chemistry West et al.[19], and purification operations in metallurgy Moffatt et al.[20]. Additionally, the growing demand for renewable energy systems in the 21st century has sparked interest in MHD energy generators, including innovative designs like liquid metal ocean wave systems Zhao et al.[21], gallium hybrid generators Niu et al. [22], bioinspired space pumps Akbar et al.[23], and nanoengineering solar MHD pumps Prakash[24]. Mathematical models play a crucial role in optimizing these designs and characterizing system performance Cramer[25], driving significant interest in theoretical and numerical simulations of MHD energy generators. Particularly in the near-wall zone of MHD generators, boundary layer models are valuable for assessing transport characteristics. In Hall MHD generators, a cross-flow is induced, and when the system rotates, Coriolis effects must be considered. Several researchers have explored the influence of Hall currents on transport characteristics, such as the work by Seddeek on non-Newtonian transport [26] and Bég on micropolar thermo-fluid transport [27]. They observed that primary flow is assisted near the wall with increasing Hall parameter whereas it is impeded further from the wall. They also showed that temperature and thermal boundary layer thickness are decreasing with increasing Hall current.

Bhatti et al. [28] studied wall slip, radiative heat flux, and cross-diffusion effects on ferric oxide ($Fe_3O_4-water$). [29–32] analyzed thermal radiation efficiency using advanced nanocomposite flow on a Riga plate, while employing numerical and intelligent neuro-computational modelling with Fourier's energy and Fick's mass flux theory for 3D fluid flow through a stretchable surface. Gomathy and Kumar [33] analogous effect of concentration gradients influencing the energy flux and the temperature field as the Dufour effect (diffuso-thermal effect). Postelnicu [34] examined the hydromagnetic free convection heat and mass transfer in a porous medium with Soret and Dufour effects. He noted that with increasing Soret number, the mass transfer rate to the wall (Sherwood number) is decreased. Makinde [35] analyzed the mixed convective MHD flow in porous media with cross-diffusion effects. He observed that local skin friction is boosted by the Soret and Dufour effects whereas the Dufour number weakly enhances concentration and species boundary layer thickness but reduces Sherwood number. [36, 39] developed the artificial neural network approach to predict thermal transport of nanofluids inside a porous enclosure. Further studies of magnetohydrodynamic convection with Soret and/or Dufour effects have been communicated by Sheri et al. [40], and Bég et al. [41].

One vital concern in MHD generator operation is the control of corrosion effects on

electrode walls, as significant corrosion can reduce efficiency and electrode lifetimes Koester and Perkins[42]. The inclusion of chemical reactions in mathematical models has garnered significant interest, in the study of both homogeneous and heterogeneous reactions. For instance, Abdallah [43] examined the collective effects of Hall current, chemical reactions, and cross diffusion on thermo-solutal transport. Makinde and Olanrewaju [44] employed an n^{th}-order Arrhenius irreversible chemical reaction model to simulate mixed convection. Kandasamy et al. [45] used Gill's decomposition method to study reactive thermo-solutal magneto-convective boundary layer flow.
Inspection of the literature has revealed that currently the collective effects of heat generation/absorption, Hall current, rotations, oscillating wall effects and non-Newtonian working fluids have not been addressed in the literature. Previous models have considered only aspects of these phenomena e.g. heat source/sink Seth et al.[46], Hall current and rotationSeth et al. [47] and oscillating effects kataria et al.[48]. Furthermore, the emergence of novel electroconductive polymeric fluent media (magneto-rheological fluids) Mantripragada et al.[49] has opened up a new era in MHD generator system design wherein smart features can now be embedded into functionality of the working fluid. With resspect to this development, the current study also implements a viscoplastic Casson model for the working fluid [50–52]. Additionally, oscillation effects of the generator wall are considered since these have been shown to provide an excellent advantage in actual power generation applications using pulsation [53, 54].
The literature review reveals a gap in addressing the collective effects of heat generation/absorption, Hall current, rotation, oscillating wall effects, and non-Newtonian working fluids. Previous models have considered aspects of these phenomena separately. Furthermore, the emergence of electro-conductive polymeric fluid media has opened up new possibilities in MHD generator system design. The current study aims to fill this gap by amalgamating multiple effects considered separately in existing models to create a comprehensive multi-physical model of rotating, oscillating wall, Hall current MHD generator flow dynamics[55–58]. This model encompasses heat and mass transfer, Soret cross diffusion, radiative flux, porous media, and ramped wall temperature physics Nandkeoiyar et al.[59]. The Darcy model is used for porosity drag force, approximating filtration materials in hybrid MHD generators Ghosh et al.[60]. The governing equations are converted into a system of ordinary differential equations and solved using the Laplace transform technique. MATLAB is employed for numerical evaluation and validation against previous studies.

2 Mathematical Formulation

The unsteady MHD free thermo-solutal convective flow of an electrically convective, incompressible, viscoplastic fluid from a vertical oscillating rotating plate in an MHD generator configuration was considered. A chemical reaction is assumed to occur. The fluid is optically thin and a unidirectional radiative flux (q_r) is present transverse to the wall. Heat absorption/generation is also assumed to occur. Thermo-diffusive flux is also present (Soret effect) in which temperature gradients influence the concentration field. Assuming Hall currents are present, the generalized Ohm's law may be stated in the following form,

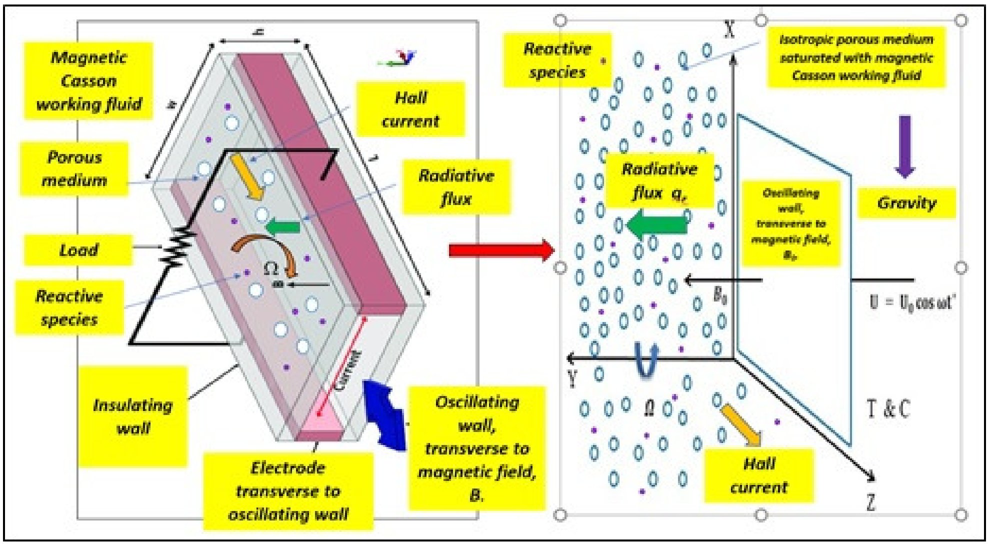

Fig. 1 Rotating hydromagnetic non-Newtonian oscillating plate in porous mediumon on the left (3-D rendition of rotating MHD generator), right- oscillating wall model

$$J = \frac{\sigma}{1+m^2}(\overline{E} + \overline{V} \times \overline{B} - \frac{1}{\sigma n_e} \times \overline{B}) \tag{1}$$

The constitutive equation for the Casson fluid can be written as,

$$\tau_{ij} = \begin{cases} 2(\mu\beta + \frac{py}{2\sqrt{\pi}})e_{ij}, \pi > \pi_e \\ 2(\mu\beta + \frac{py}{2\sqrt{\pi_e}})e_{ij}, \pi < \pi_e \end{cases} \tag{2}$$

The coordinate system is shown in Fig.(1). The plate lies in the XZ plane with the Y-axis normal to it. The fluid and oscillating wall (plate) spin in unison in the counterclockwise direction with angular velocity Ω about the Y-axis. At $t^* \leq 0$, the fluid and the plate are both at rest at T_∞ and C_∞. At time $t^* > 0$, the wall temperature is modified to $T_\infty + (T_w - T_\infty)^{\frac{t^*}{t_0}}$ when $t^* \leq t_0$ and constant temperature is sustained of T_w when $t^* > t_0$. Also, the surface concentration of reactive species is increased to $C_\infty + (C_w - C_\infty)^{\frac{t^*}{t_0}}$, when $t^* \leq t_0$ and constant concentration is present(C_w) when $t^* \geq t_0$. For the concentration equation, the Soret effect is taken into account. According to the above assumptions the boundary layer equation extending the model in Patel[51] is as follows:

$$\frac{\partial U}{\partial Y} = 0 \tag{3}$$

$$\frac{\partial U}{\partial t^*} + 2\Omega W = \mu_\beta \left(1 + \frac{1}{\gamma}\right)\frac{\partial^2 U}{\partial Y^2} - \frac{\sigma B_0^2}{(1+m^2)}(U + mW) + g\rho\beta_T(T - T_\infty) + g\rho\beta_C(C - C_\infty) - \frac{\mu_\beta U}{k}, \tag{4}$$

$$\frac{\partial W}{\partial t^*} - 2\Omega U = \mu_\beta \left(1 + \frac{1}{\gamma}\right) \frac{\partial^2 W}{\partial Y^2} + \frac{\sigma B_0^2}{(1+m^2)}(W - mU) - \frac{\mu_\beta U}{k}, \tag{5}$$

$$\frac{\partial T}{\partial t^*} = \frac{k}{\rho C_p} \frac{\partial^2 T}{\partial Y^2} + \frac{Q_0}{\rho C_p}(T - T_\infty) - \frac{1}{\rho C_p} \frac{\partial q_r}{\partial Y}, \tag{6}$$

$$\frac{\partial C}{\partial t^*} = D_M \frac{\partial^2 C}{\partial Y^2} - k_2(C - C_\infty) + \frac{D_M K_T}{T_M} \frac{\partial^2 T}{\partial Y^2}. \tag{7}$$

The imposed spatial and temporal boundary conditions are as follows:

$$\begin{gathered} U = 0, \quad W = 0, \quad T = T_\infty, \quad C = C_\infty, \quad as \quad Y \geq 0 \quad and \quad t^* \leq 0, \\ U = U_0 cos\omega t^*, W = 0, T = \begin{cases} T_\infty + (T_w - T_\infty)\frac{t^*}{t_0}, & 0 < t^* < t_0 \\ T_w \quad , & t^* \geq t_0, \end{cases} \\ C = C_\infty + (C_w - C_\infty)\frac{t^*}{t_0}, \quad at \quad Y = 0 \quad and \quad t^* \geq 0, \\ U \to 0, \quad T \to T_\infty, \quad C \to C_\infty \quad as \quad Y \to \infty \quad and \quad t^* \geq 0. \end{gathered} \tag{8}$$

The radiative heat flux is given by the algebraic Rosseland diffusion approximation:

$$q_r = -\frac{4\sigma^*}{3k^*} \frac{\partial T^4}{\partial y}, \tag{9}$$

By applying the Taylor series expansion to T_∞ and neglecting higher-order terms we have:

$$T^4 = 4T_\infty^3 T - 3T_\infty^4, \tag{10}$$

The radiative flux term therefore becomes:

$$\frac{\partial q_r}{\partial Y} = \frac{16\sigma^* T_\infty^3}{3k^*} \frac{\partial^2 T}{\partial Y^2}. \tag{11}$$

We define the following nondimensional quantities:

$$\begin{gathered} u = \frac{U}{U_0}, w = \frac{W}{U_0}, y = \frac{YU_0}{\nu}, t = \frac{t^* U_0^2}{\nu}, \theta = \frac{T - T_\infty}{T_w - T_\infty}, \phi = \frac{C - C_\infty}{C_w - C_\infty}, K = \frac{\Omega v}{U_0^2}, \\ Gr = \frac{\gamma g \beta_T (T - T_\infty)}{U_0^3}, M^2 = \frac{\sigma B_0^2 v}{\rho U_0^2}, Gm = \frac{\gamma g \beta_C (C - C_\infty)}{U_0^3}, K_2 = \frac{\gamma k_2}{U_0^2}, Rd = \frac{16 a^* \sigma^* \gamma T_\infty}{U_0^2 \rho C_p}, \\ K_1 = \frac{k U_0^2}{\nu^2}, Q = \frac{Q_0 v}{U_0^2 \rho C_p}, Pr = \frac{\rho \nu C_p}{k}, Sc = \frac{\nu}{D_m}, So = \frac{D_M K_T}{T_M \nu} \frac{(T_w - T_\infty)}{(C_w - C_\infty)}. \end{gathered} \tag{12}$$

By substituting Eqn.(12) into (4)-(7) with the modified expression for radiative flux from (11), the following system of dimensionless conservation equations is obtained:
Primary momentum (x)

$$\frac{\partial u}{\partial t} + 2K^2 w = \left(1 + \frac{1}{\gamma}\right) \frac{\partial^2 u}{\partial y^2} - \frac{M^2}{(1+m^2)}(u + mu) + Gr\theta + Gm\phi - \frac{u}{K_1}, \tag{13}$$

Secondary momentum (z)

$$\frac{\partial w}{\partial t} - 2K^2 u = \left(1 + \frac{1}{\gamma}\right)\frac{\partial^2 w}{\partial y^2} + \frac{M^2}{(1+m^2)}(w - mu) - \frac{w}{K_1}, \tag{14}$$

Energy Equation:

$$\frac{\partial \theta}{\partial t} = \frac{1}{Pr}\frac{\partial^2 \theta}{\partial y^2} + \left(Q - \frac{Rd}{Pr}\right)\theta, \tag{15}$$

Species Concentration Equation:

$$\frac{\partial \phi}{\partial t} = \frac{1}{Sc}\frac{\partial^2 \phi}{\partial y^2} + So\frac{\partial^2 \theta}{\partial y^2} - K_2\phi. \tag{16}$$

The associated boundary conditions (8) assume the following form:

$$\begin{aligned} &u = w = \theta = \phi = 0, \quad if \quad y \geq 0, t \leq 0, \\ &u = cos(\omega t), \quad w = 0, \quad \theta = \left\{ t, 0 < t \leq 1, t > 0 \right\} = tH(t) - (t-1)H(t-1), \\ &\quad \phi = t, at \quad y = 0, t > 0, \\ &u, w, \theta, \phi \to 0, \quad at \quad y \to \infty, t > 0. \end{aligned} \tag{17}$$

By virtue of complex variables, the primary (u) and secondary (w) velocity components can be homogenized into a single velocity function, $F = u + iw$. Introducing this in the momenta Eqns. (13)-(14), we obtain the contracted version:

$$\frac{\partial F}{\partial t} + \left(\frac{M^2(1 - im)}{1+m^2} + \frac{1}{K_1} - 2ik^2\right)F = \left(1 + \frac{1}{\gamma}\right)\frac{\partial^2 F}{\partial y^2} + Gr\theta + Gm\phi \tag{18}$$

The boundary conditions (17) now emerge as:

$$\begin{gathered} F = 0, \theta = 0, \phi = 0 \quad if \quad y \geq 0, t \leq 0, \\ F = cos(\omega t), \theta = \begin{Bmatrix} t, 0 < t \leq 1 \\ 1, t > 0 \end{Bmatrix} = tH(t) - (t-1)H(t-1), \phi = t, at \quad y = 0, t > 0, \\ F, \theta, \phi \to 0, \quad at \quad y \to \infty, t > 0. \end{gathered} \tag{19}$$

3 Method of Solution

Eqns. (18), (15), (16) with conditions (19) are solved analytically by the Laplace transform technique. The exact solutions for $F(y,t)$,$\theta(y,t)$ and $\phi(y,t)$ emerge as follows:

$$\theta(y,t) = (1-e^{-s})\tfrac{1}{2}exp(y\sqrt{Pr(Rd+Q)}erfc\left(\tfrac{y}{2}\tfrac{\sqrt{Pr}}{\sqrt{t}} + \sqrt{\tfrac{Pr(Rd+Q)t}{Pr}}\right)$$

$$+\frac{1}{2}exp(-y\sqrt{Pr(Rd+Q)}erfc\left(\frac{y}{2}\frac{\sqrt{Pr}}{\sqrt{t}} - \sqrt{\frac{Pr(Rd+Q)t}{Pr}}\right), \quad (20)$$

$$\phi(y,t) = \tfrac{1}{2}exp(y\sqrt{K_2Sc}erfc\left(\tfrac{y}{2}\tfrac{\sqrt{Sc}}{\sqrt{t}} + \sqrt{K_2}t\right)$$

$$+\frac{1}{2}exp(-y\sqrt{K_2Sc}erfc\left(\frac{y}{2}\frac{\sqrt{Sc}}{\sqrt{t}} + \sqrt{K_2}t\right), \quad (21)$$

$$F(y,t) = \tfrac{1}{2}f_1(y,t) + \tfrac{1}{2}f_2(y,t) + a_{31}f_8(y,t) + a_{32}f_9(y,t) + a_{33}f_{10}(y,t)$$
$$+ a_{30}f_{11}(y,t) + (a_{18}+a_{19})f_{12}(y,t) + (a_{22}-a_{25}-a_{26})f_{13}(y,t) - a_{29}f_5(y,t)$$
$$+ (a_{18}+a_{19})f_{16}(y,t) - a_{30}f_5(y,t) + g_3(y,t) - g_3(y,t-1)H(t-1) + g_4(y,t)$$
$$+g_4(y,t-1)H(t-1) - (a_{18}-a_{15})f_2(y,t) - (a_{21}+a_{23}+a_{28})f_4(y,t)$$

$$+a_{19}f_{16}(y,t) - (a_{22}+a_{25}+a_{26})f_{17}(y,t) - a_{27}f_6(y,t). \quad (22)$$

Here all algebraic functions a_1, b_1, c_1, d_1, etc are defined in the Appendix.

3.1 Solution to the Problem for Isothermal Temperature

To understand the effects of the ramped temperature of the plate on the fluid flow, we must compare our results with constant temperature. In this case, the initial and boundary conditions are used. The special case of an isothermal plate is retrieved when we set $\theta = 1$ at $y = 0$ and $t \geq 0$. For this case we have:

$$\theta(y,t) = f_4(y,t) - f_4(y,t-1)H(t-1), \quad (23)$$

$$\phi(y,t) = a_5f_6(y,t) - a_5(f_4(y,t) + f_4(y,t-1)H(t-1)), \quad (24)$$

$$F(y,t) = \frac{1}{2}f_1(y,t) + \frac{1}{2}f_2(y,t) - a_{29}f_4(y,t) + a_{18}f_4(y,t) + a_{29}f_6(y,t) + a_{18}f_6(y,t). \quad (25)$$

4 Wall Gradient Characteristics

In an MHD energy generator near wall flows, the key characteristics for designers are the wall shear stress, heat transfer rate (Nusselt number) and wall mass transfer rate (Sherwood number). These are evaluated using Eqns. (23)-(25). The dimensional wall shear stress (skin friction) takes the form:

$$\tau_{cos}(y,t) = -\mu_\beta\left(1+\frac{1}{\gamma}\right)\left(\frac{\partial u}{\partial y}\right)_{y=0}, \quad (26)$$

Table 1 Comparison study of $f''(0)$, when $So = Q = Rd = 0$ for various values of γ,K,M,K_1

γ	K	M	K_1	Patel[51] Ramped	Isothermal	Present Study Ramped	Isothermal	R-K method Ramped	Isothermal
0.1	0.2	0.1	1	-0.4813	-0.4779	-0.4902	-0.4801	-0.4809	-0.4724
0.15	0.2	0.1	1	-0.3481	-0.4018	-0.3625	-0.4112	-0.3584	-0.4051
0.1	0.3	0.1	1	-0.5503	-0.4807	-0.5701	-0.4890	-0.5817	-0.4635
0.1	0.4	0.1	1	-0.6194	-0.4834	-0.6207	-0.4841	-0.6156	-0.4608
0.1	0.2	0.3	1	-0.4475	-0.4502	-0.4561	-0.4590	-0.4649	-0.4651
0.1	0.2	0.4	1	-0.5284	-0.5165	-0.5310	-0.5215	-0.5313	-0.5247
0.1	0.2	0.1	1.1	-0.5891	-0.5765	-0.5902	-0.5811	-0.5919	-0.5813
0.1	0.2	0.1	1.2	-0.6966	-0.6735	-0.7051	-0.6881	-0.6907	-0.6802

The nondimensional skin friction by virtue of Eqn.(23) emerges for the isothermal case as:

$$\tau_{cos}(y,t) = \frac{1}{2}f_1(t + \frac{1}{2}f_2(t) - a_{29}f_4(t)) - a_{18}f_4(t) + a_{29}f_6(t) + a_{18}f_6(t), \tag{27}$$

The Nusselt number can be defined as:

$$Nu(y,t) = -Rd\left(\frac{\partial T}{\partial y}\right)_{y=0}, \tag{28}$$

For the ramped temperature case, the appropriate expression using Eqn. (23) is:

$$Nu(y,t) = -(f_5(t) - f_5(t-1)H(t-1)), \tag{29}$$

For the isothermal wall case, we have:

$$Nu(y,t) = -(f_4(t)), \tag{30}$$

The Sherwood number can be defined as:

$$Sh(y,t) = -\left(\frac{\partial C}{\partial y}\right)_{y=0}, \tag{31}$$

For the isothermal case we have:

$$Sh(y,t) = a_5f_6(t) - a_5(f_4(t) + f_4(t-1) + H(t-1)). \tag{32}$$

5 Results and Discussion

In this research, we have successfully obtained exact solutions for oscillating Magneto-hydrodynamic (MHD) Casson transport from a vertical plate next to a Darcian porous

Table 2 Variations study of the Skin friction for various values of t, ν and K_1

t	ν	K_1	Skin friction Ramped	Skin friction Isothermal
0.4	0.1	1.5	-3.6675	-5.9465
0.5	0.1	1.5	-2.7520	-5.60734
0.4	0.2	1.5	-2.5823	-4.3865
0.4	0.3	1.5	-2.1426	-3.7276
0.4	0.1	1.6	-1.7803	-3.5651
0.4	0.1	1.7	-1.7195	-3.6405

Table 3 Variations of the Nusselt number for various values of t and Q

t	Q	Nu
0.4	0.7	0.25508
0.4	0.8	0.27946
0.5	0.5	0.25609
0.6	0.5	0.30149

Table 4 Variations of the Sherwood number for various values of t and K_2

t	K_2	Sh
0.4	1.1	0.16614
0.4	1.2	0.17487
0.6	1	0.23987
0.7	1	0.28297

medium. This study revealed various significant effects, such as chemical reactions, heat source/sink, ramped wall temperature, and Soret effects. To perform numerical evaluations, we utilized MATLAB symbolic software. Our choice of parameters, including Grashof number (Gr), time (t), Prandtl number (Pr), Reynolds number (Re), heat generation parameter (Q), Schmidt number and Soret effects (Sc and So), magnetic field (M), Casson viscoplastic parameter (γ), and rotational parameter, aligns with real-world rotating MHD operation devices, as documented in references[53, 54]. To obtain representative plots for actual working fluids, a default value of the Pr is taken as 0.71 (air), and Sc is selected as 0.6. This section presents a detailed examination of the physical behavior of various factors, changing only one variable whose influence is being researched while keeping the other parameters constant, such as $Pr = 0.7$; $M = 0.1$; $K = 0.5$; $K_1 = 2$; $So = 0.2$; $Q = 0.5$; $w = 0.3$; $\gamma = 0.2$; $Gr = 0.3$; $m = 2$; $Rd = 0.5$; $K_2 = 1$; $Sc = 0.2$; $t = 1$. The results are presented in Tables 1, which provide valuable comparisons. Notably, the skin friction is consistently higher for the ramped wall temperature case compared to the isothermal case are shown Table 1. Table 2-4 shows that variation of skin frction, the rate of heat and mass transfer. By increasing the heat source parameter from 0.7 to 0.8 increases the heat transfer rate by 9.5% and increasing the chemical reaction parameter from 1.1 to 1.2 increases the mass transfer rate by 5.2%. The flow characteristics are further illustrated in Figures

(2)(a-e). In Fig.(2)(a), we observe the evolution of the velocity with transverse coordinates under various parameters. An increase in the magnetic field (M) evidently leads to a decrease in velocity function (F). Compared with the isothermal case, ramped wall temperature case achieves lower velocity magnitudes, suggesting improved flow control with a constant temperature along the oscillating plate. An increase in the magnetic field strength enhances the magnetic forces acting on the fluid, which can suppress fluid motion and momentum. This effect is particularly pronounced in MHD flows, where the Lorentz force induced by the magnetic field interacts with the fluid velocity, leading to a reduction in flow velocities. Fig.(2)(b) illustrates that incrase in the Hall parameter has the oppsite effect on the magnetic body force parameter, m. The homogenized velocity is increased strongly. The overall effect is therefore acceleration, and a thinner momentum boundary layer thickness will be produced. The Hall current can therefore achieve a compensatory role in MHD generator operations and the complex flow field can be manipulated very effectively. It is noteworthy that with variation in Hall parameter however, there is no tangible deviation between the ramped and isothermal plate cases. In both cases the behaviour of velocity at the wall is the same, unlike in the case of magnetic parameter variation, m. Fig.(2)(c) reveals that with greater values of Casson viscoplastic parameter, γ, there is a significant deceleration in the flow. Larger values of this parameter inhibit momentum development since the magnetic non-Newtonian fluid requires greater shear for mobilization. The isothermal plate case again achieves higher magnitudes of velocity. Casson fluids generally offer more resistance to deformation compared to Newtonian fluids. As viscosity increases, the fluid becomes more resistant to flow and deformation, resulting in lower velocities under similar flow conditions. Fig.(2)(d) shows that with greater values of the rotational parameter, K, there is a decrease in linear velocity in the regime. The supplementary angular momentum swamps the development of primary (and secondary) momentum with greater rotational velocity. This leads to strong deceleration and a thicker momentum (hydrodynamic) boundary layer thickness. Fig.(2)(e) indicates that with greater values of the permeability parameter, K_1, there is a strong escalation in velocity. Increased permeability allows fluid particles to move more easily through the porous medium. This enhanced mobility enables the fluid to traverse the medium more quickly, leading to higher velocities.

In Fig.(3)(a) a substantial decrease in temperature is produced with greater Prandtl number. This phenomenon is often observed in situations involving low Pr fluids, like air, when it flows over a hot or cold surface. The temperature gradient near the surface is pronounced, and the temperature decreases rapidly away from the surface due to the efficient conduction of heat. The isothermal case produces temperatures which supercede the ramped wall temperature case, notably at the wall. Fig.(3)(b) demonstrates that with a stronger heat source (generation) there is a noticeable increase in temperatures. The supplementary thermal energy clearly encourages enhanced thermal diffusion in the boundary layer. Much lower magnitudes of temperature are obtained for the ramped wall case indicating that this appraoch is preferable for cooling the regime. Heating of the regime is achieved with the isothermal case, again most prominently at the oscillating wall. Fig.(3)(c) shows that an increase in radiative

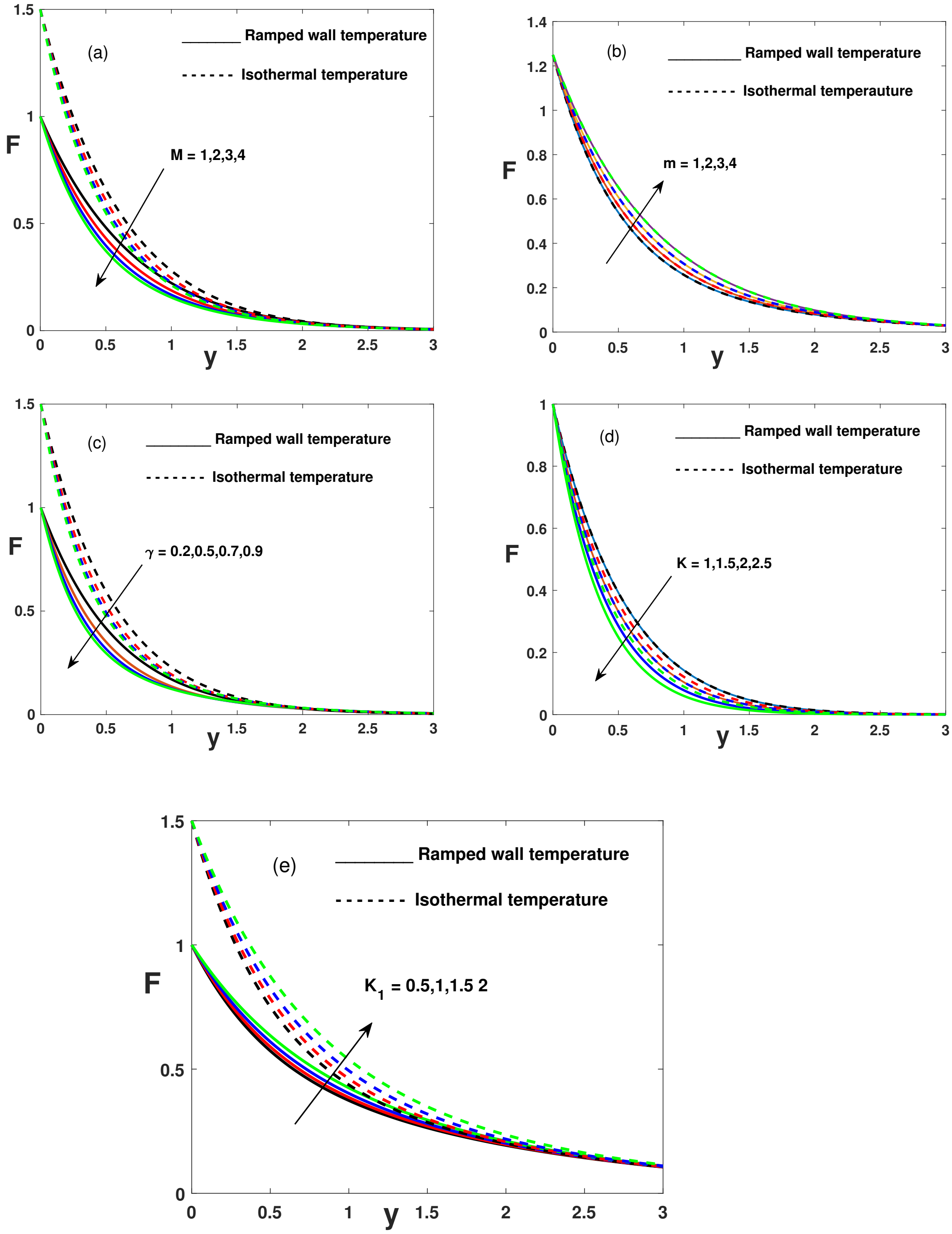

Fig. 2 Velocity profiles for f versus y, (a) Magnetic field, (b) Hall current parameter, (c) Casson fluid, (d) Rotating parameter, (e) Permeability parameter.

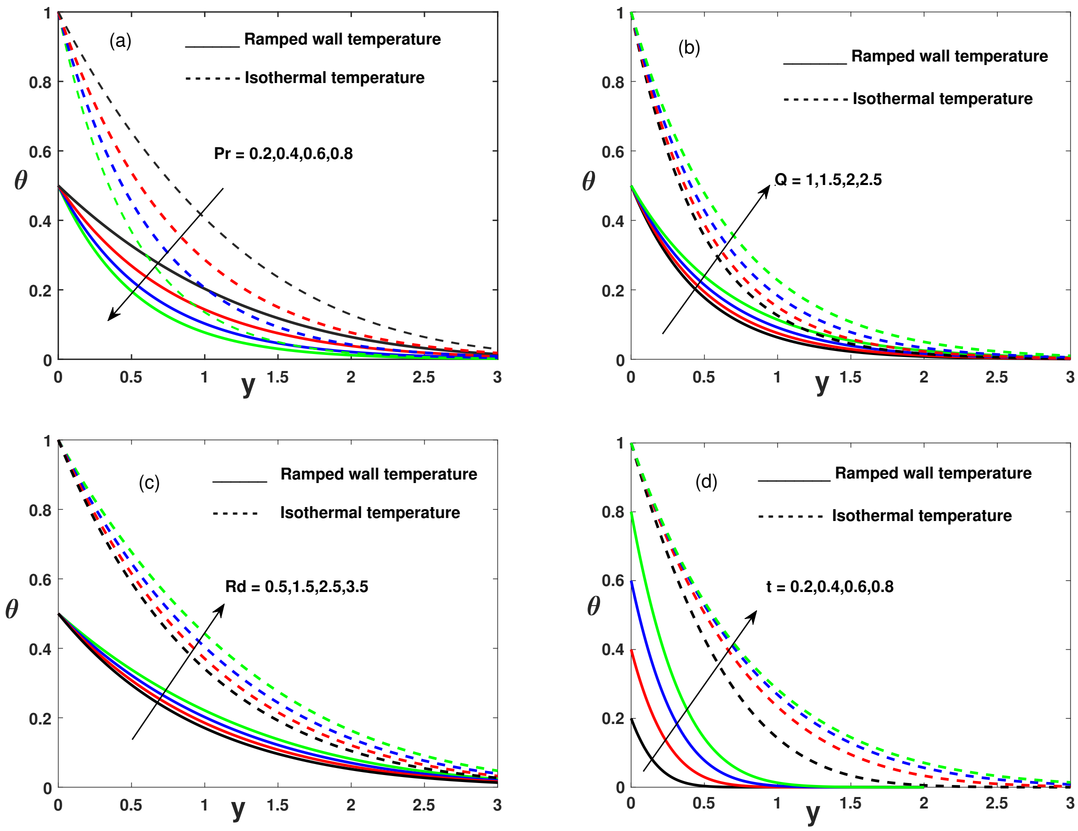

Fig. 3 Temperature profiles for θ versus y, (a) Prandtl number, (b) heat source/sink, (c) radiation parameter, (d) time.

parameter, Rd, induces a strong heating effect in the regime. The magnetic Casson fluid is energized by stronger radiative flux. Thermal boundary layer thickness is increased. If the radiative flux effect is neglected temperatures will be under-predicted. The ramped wall case attains much lower temperatures relative to the isothermal case. The implication is that undesirable high temperatures induced by radiative flux may be controlled via ramping of the heat condition imposed at the oscillating wall. Fig.(3)(d) shows that very strong reduction in temperature is present at low times; as time progresses thermal diffusion is enabled and temperatures are able to ascend significantly in the boundary layer transverse to the oscillating plate. Temperature gradient at the wall is also significantly reduced with progression in time and the temperature plots morph from sharp descents to monotonic decays in the free stream. Significantly lower temperatures again correspond to the ramped wall case relative to the isothermal case.

Fig.(4)(a) shows that with increasing in Soret number, So, there is a considerable reduction in concentration magnitudes. In all cases asymptotically smooth profiles are achieved from the oscillating wall ($y = 0$) to the free stream i. e. edge of the boundary layer. The concentration flux is inhibited by temperature gradient due to Soret thermo-diffusion (in the concentration equation i. e. the term $So\ \frac{\partial^2\theta}{\partial y^2}$), and this reduces the species concentration boundary layer thickness. Fig.(4)(b) shows that with stronger first order destructive chemical reaction parameter,K_2, there is a noticeable reduction in species concentration. The greater intensity of chemical reaction converts more of the original species into a new species, which leads to a depletion in the original species concentration. Concentration boundary layer thickness will also be suppressed. Fig.(4)(c) reveals that with increment in Schmidt number the concentration magnitudes are also depleted strongly.this phenomenon is often observed in situations involving low Schmidt number fluids, like water (Sc is low for dissolved gases in water), when it flows over a surface that introduces or removes a solute. The concentration gradient near the surface is not as pronounced, and the concentration decreases more slowly away from the surface due to the inefficient mass diffusion. Fig.(4)(d) it is evident that with progression in time, species concentration is significantly enhanced throughout the boundary layer regime. Concentrations are always a maximum at the wall and decay to zero in the free stream. With increment in time, the concentration gradient is also boosted at the wall. Species boundary layer thickness grows with time in the regime. Figs.(5)-(6) shows the impact of streamlines when $\gamma = 0.5, 0.7$, $K = 1.0, 2.0$. In Fig. (5), when the Casson fluid increases in a flow field, it leads to an increase in the streamline value because of the accelerated flow and the greater centripetal acceleration by fluid particles as they follow the curved flow path. In Fig. (6), when increasing the rotational parameter values in a fluid flow, the behavior of the streamlines can be affected significantly. Specifically, with increasing rotational parameters, the fluid flow tends to exhibit a more rotational or swirling motion. This implies that the streamlines become more curved and start to form vortex patterns within the flow. As the rotational effects become more pronounced, the streamlines tend to wrap around the central axis, forming distinct whirlpool-like structures, thereby indicating a stronger rotational component in the fluid dynamics.

6 Conclusions

In conclusion, this research provides a comprehensive exploration of hydromagnetic free convective thermosolutal transport in Casson fluid flow from a rotating vertical wall to a permeable medium with the Soret effect. The PDEs relevant to fluid fow are transformed into coupled non-linear ODEs using the nondimensional quantities. The mathematical model incorporates radiative flux, heat source/sink, and chemical reaction effects and is solved using a Laplace transform technique in MATLAB. The findings of this study reveal critical insights:

- Velocity profile increases with m and K_1 and greater velocity magnitudes are obtained for isothermal case than for the ramped wall temperature case.
- Velocity is depleted with greater M, γ, K with a correspondingly larger momentum boundary layer thickness.

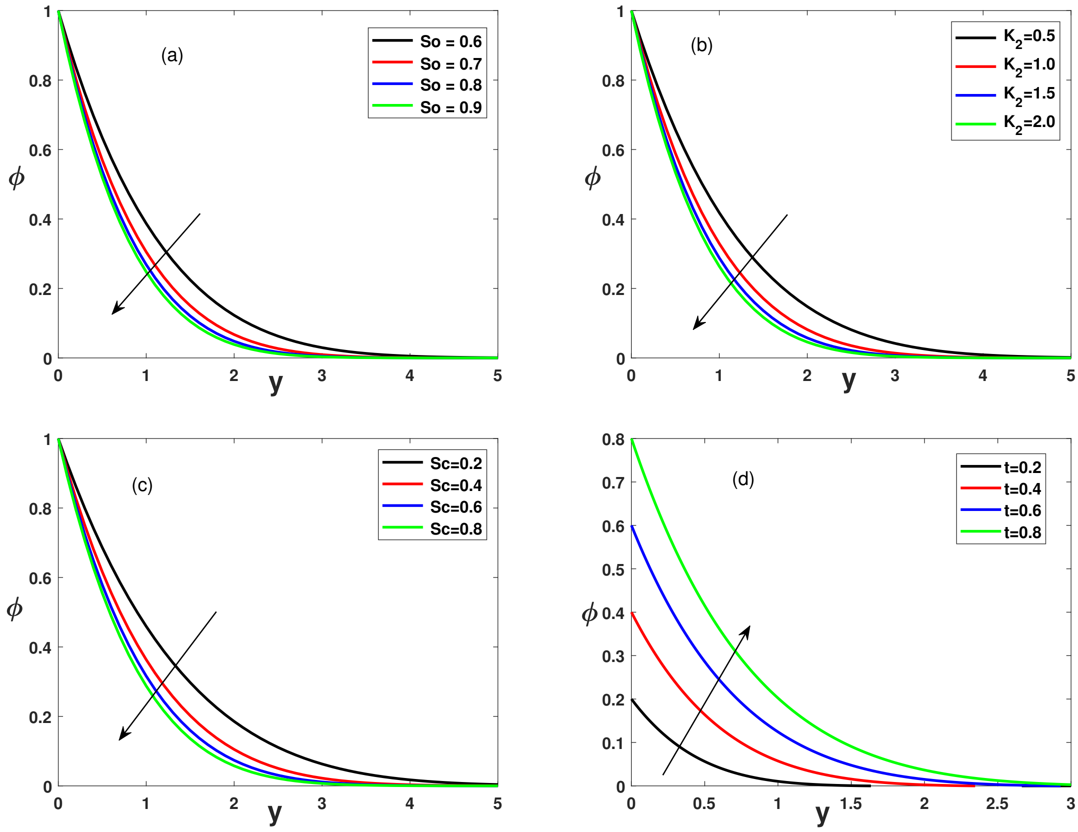

Fig. 4 Concentration profiles for ϕ versus y, (a) soret parameter, (b) chemical reaction, (c) Schmidt number, (d) time.

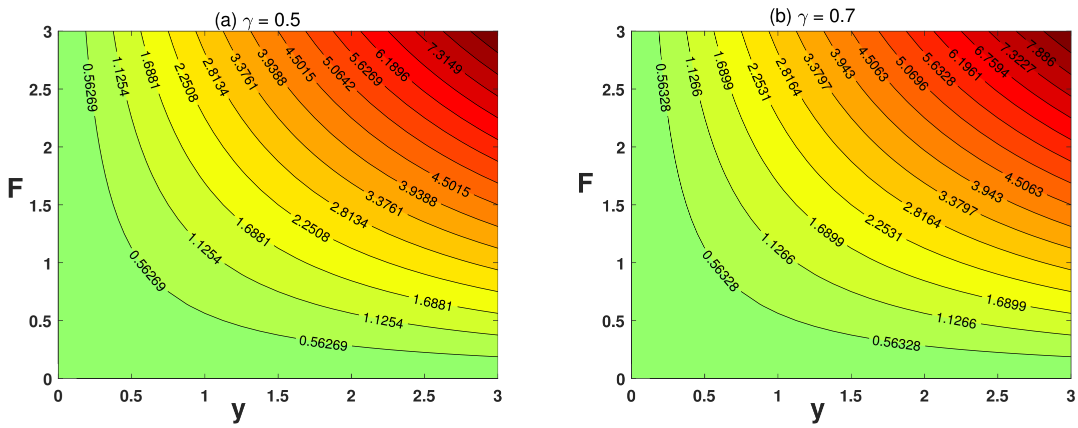

Fig. 5 Streamlines for (a) $\gamma = 0.5$, (b) $\gamma = 0.7$

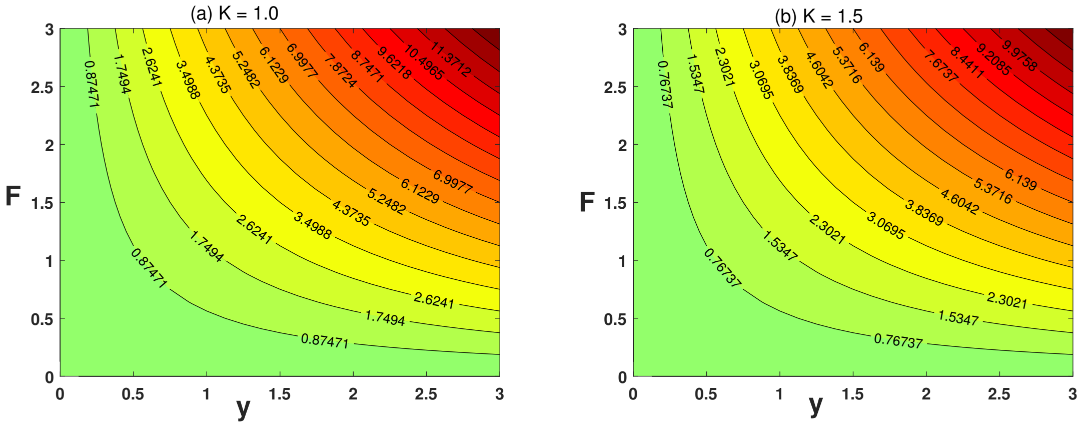

Fig. 6 Streamlines for (a) $K = 1.0$, (b) $K = 1.5$

- Temperature magnitudes, thermal boundary layer thickness increase with Rd, Q, and t. Moreover, in the isothermal wall case, higher temperature values are computed compared to the ramped wall temperature case.
- Concentration magnitudes and species boundary layer thickness decrease with an increase in So, Sc, and K_2. Conversely, an increase in time leads to the opposite effect.
- By increasing the Q from 0.7 to 0.8 increases the heat transfer rate by 9.5% and increasing the K_2 from 1.1 to 1.2 increases the mass transfer rate by 5.2%.

This research sheds light on the near-wall boundary layer characteristics of rotating MHD generators, yet it's essential to acknowledge that the study does not encompass complex effects like Dufour, Future investigations should consider these factors, especially in scenarios with high magnetic Reynolds numbers.

Appendix

$a_1 = R - Sc.K, a_2 = Pr - Sc, a_3 = \frac{a_1}{a_2}, R = (Q - \frac{Rd}{Pr}), a_5 = \frac{1}{a_3 a_2}, a_6 = \frac{1}{a_2 a_3^2},$
$b_1 = R - \frac{\alpha}{j}, b_2 = Pr - \frac{1}{j}, b_3 = \frac{b_1}{b_2}, c_1 = ScK - \frac{\alpha}{j}, c_2 = Sc - \frac{1}{j}, c_3 = \frac{c_1}{c_2},$
$d_1 = R - \frac{\alpha}{j}, a_4 = So.Sc(\frac{1}{a_2(1+a_3)} - \frac{1}{a_2 a_3} - \frac{1}{a_2 a_3^2(1+a_3)}), d_2 = Pr - \frac{1}{j}, d_3 = \frac{d_1}{d_2},$
$a_7 = Gr\left(\frac{1}{b_2(1+b_3)} - \frac{1}{b_2 b_3} - \frac{1}{b_2 b_3^2(1+b_3)}\right), a_8 = \frac{Gr}{b_2 b_3}, a_9 = \frac{Gr}{b_2 b_3^2},$
$a_{10} = -So.Sc\left(\frac{1}{a_2(1+a_3)} + \frac{1}{a_2 a_3} + \frac{1}{a_2 a_3^2(1+a_3)}\right), a_{11} = \frac{Gm(1+a_5)}{c_2 c_3},$
$a_{12} = \frac{Gm(1+a_5)}{c_2 c_3^2}, a_{13} = -\frac{Gm(1+a_8)}{c_2}\left(\frac{1}{1+c_3} - \frac{1}{c_3} - \frac{1}{c_3^2(1+c_3)}\right), a_{14} = \frac{Gma_6}{c_2(c_3+a_3)},$
$a_{15} = \frac{Gma_4}{d_2 d_3}, a_{16} = (\frac{1}{d_2(1+d_3)} - \frac{1}{d_2 d_3} - \frac{1}{d_2 d_3^2(1+d_3)}), a_{17} = \frac{Gma_5}{d_2 d_3},$
$a_{18} = -\frac{Gma_5}{d_2 d_3^2}, a_{19} = \frac{-Gma_6}{d_2(a_3+d_3)}, a_{20} = \frac{-Gma_6}{d_2(a_3+d_3)}, a_{21} = \frac{Gma_{10}}{d_2 d_3}, a_{22} = \frac{Gma_{10}}{d_2 d_3^2},$
$a_{24} = \frac{Gma_{11}}{d_2 d_3}, a_{23} = \frac{Gma_{11}}{d_2}\left(\frac{1}{1+d_3} - \frac{1}{d_3} - \frac{1}{d_3^2(1+d_3)}\right), a_{25} = \frac{Gma_{11}}{d_2 d_3^2}, a_{26} = \frac{Gma_{12}}{d_2(a_3+d_3)},$
$a_{27} = (a_{13}+a_{17}+a_{21}-a_{23}), a_{28} = (a_{21}+a_{15}), a_{29} = (a_{16}+a_{20}-a_{27}), a_{30} = (a_{29}+a_{15}),$

$$\alpha=\left(\frac{M^2(1-im)}{1+m^2}+\frac{1}{k}-2ik^2\right), a=1, b=j,$$
$$f_1(y,t)=\frac{exp(iwt)}{2}\left(exp(y\sqrt{a/b+iws})erfc\left(\frac{y\sqrt{a/b}}{2\sqrt{t}}+\sqrt{\frac{a/bt}{1/b}}-iwt\right)\right.$$
$$\left.+exp(-y\sqrt{a/b+iws})erfc\left(\frac{y\sqrt{a/b}}{2\sqrt{t}}-\sqrt{\frac{a/bt}{1/b}}-iwt\right)\right),$$
$$f_2(y,t)=\frac{exp(-iwt)}{2}\left(exp(y\sqrt{a/b-iws})erfc\left(\frac{y\sqrt{a/b}}{2\sqrt{t}}+\sqrt{\frac{a/bt}{1/b}}-iwt\right)\right.$$
$$\left.+exp(-y\sqrt{a/b-iws})erfc\left(\frac{y\sqrt{a/b}}{2\sqrt{t}}-\sqrt{\frac{a/bt}{1/b}}-iwt\right)\right),$$
$$f_3(y,t)=\frac{1}{2}\left(exp(y\sqrt{a/b})erfc(\frac{y}{2\sqrt{t}}+\sqrt{a/b}t)+exp(-y\sqrt{a/b})erfc(\frac{y}{2\sqrt{t}}-\sqrt{a/b}t)\right),$$
$$f_4(y,t)=\frac{t}{2}+\frac{yPr}{4\sqrt{R}}\left(exp(y\sqrt{R})erfc(\frac{y\sqrt{Pr}}{2\sqrt{t}}+\sqrt{\frac{Rt}{Pr}})+exp(-y\sqrt{R})erfc(\frac{y\sqrt{Pr}}{2\sqrt{t}}-\sqrt{\frac{Rt}{Pr}}\right),$$
$$f_5(y,t)=\left(\frac{t}{2}+\frac{yPr}{4\sqrt{R}}\right)\left(exp(y\sqrt{R})erfc(\frac{y\sqrt{Pr}}{2\sqrt{t}}+\sqrt{\frac{Rt}{Pr}})+exp(-y\sqrt{R})erfc(\frac{y\sqrt{Pr}}{2\sqrt{t}}-\sqrt{\frac{Rt}{Pr}}\right),$$
$$f_6(y,t)=\frac{exp(-a_3t)}{2}\left(exp(y\sqrt{R-a_3Pr})erfc\left(\frac{y\sqrt{Pr}}{2\sqrt{t}}+\sqrt{\frac{Rt}{Pr}}\right)\right.$$
$$\left.-exp(-y\sqrt{R-a_3Pr})erfc\left(\frac{y\sqrt{Pr}}{2\sqrt{t}}-\sqrt{\frac{Rt}{Pr}}\right)\right),$$
$$f_7(y,t)=\frac{1}{2}\left(exp(y\sqrt{K_2Sc})erfc(\frac{y\sqrt{Sc}}{2\sqrt{t}}+\sqrt{K_2t})+exp(-y\sqrt{K_2Sc})erfc(\frac{y\sqrt{Sc}}{2\sqrt{t}}-\sqrt{K_2t}\right),$$
$$f_8(y,t)=\left(\frac{t}{2}+\frac{ySc}{4\sqrt{K_2}}\right)\left(exp(y\sqrt{K_2Sc})erfc(\frac{y\sqrt{Sc}}{2\sqrt{t}}+\sqrt{K_2t})+exp(-y\sqrt{K_2Sc})erfc(\frac{y\sqrt{Sc}}{2\sqrt{t}}-\sqrt{K_2t}\right),$$
$$f_9(y,t)=\left(\frac{exp(-a_3t)}{2}\right)\left(exp(y\sqrt{(K_2-a_3)Sc})erfc(\frac{y\sqrt{Sc}}{2\sqrt{t}}+\sqrt{(K_2-a_3)t}\right.$$
$$\left.+exp(-y\sqrt{(K_2-a_3)Sc})erfc(\frac{y\sqrt{Sc}}{2\sqrt{t}}-\sqrt{(K_2-a_3)t}\right),$$
$$f_{10}(y,t)=\left(\frac{t}{2}+\frac{y}{4\sqrt{a/b}}\right)\left(exp(y\sqrt{a/b})erfc(\frac{y}{2\sqrt{t}}+\sqrt{a/bt})+exp(-y\sqrt{a/b})erfc(\frac{y}{2\sqrt{t}}-\sqrt{a/bt}\right),$$
$$f_{11}(y,t)=\left(\frac{exp(-a_3t)}{2}\right)\left(exp(y\sqrt{(a/b-a_31/b)})erfc(\frac{y\sqrt{1/b}}{2\sqrt{t}}+\sqrt{\frac{(a/b)t}{1/b}-a_3t}\right.$$
$$\left.+exp(-y\sqrt{(a/b-a_31/b)})erfc(\frac{y\sqrt{1/b}}{2\sqrt{t}}-\sqrt{\frac{(a/b)t}{1/b}-a_3t}\right),$$
$$f_{12}(y,t)=\left(\frac{exp(-b_3t)}{2}\right)\left(exp(y\sqrt{(a/b-b_31/b)})erfc(\frac{y\sqrt{1/b}}{2\sqrt{t}}+\sqrt{\frac{(a/b)t}{1/b}-b_3t}\right.$$
$$\left.+exp(-y\sqrt{(a/b-b_31/b)})erfc(\frac{y\sqrt{1/b}}{2\sqrt{t}}-\sqrt{\frac{(a/b)t}{1/b}-b_3t}\right),$$
$$f_{13}(y,t)=\left(\frac{exp(-c_3t)}{2}\right)\left(exp(y\sqrt{(a/b-c_31/b)})erfc(\frac{y\sqrt{1/b}}{2\sqrt{t}}+\sqrt{\frac{(a/b)t}{1/b}-c_3t}\right.$$
$$\left.+exp(-y\sqrt{(a/b-c_31/b)})erfc(\frac{y\sqrt{1/b}}{2\sqrt{t}}-\sqrt{\frac{(a/b)t}{1/b}-c_3t}\right),$$
$$f_{14}(y,t)=\left(\frac{exp(-d_3t)}{2}\right)\left(exp(y\sqrt{(a/b-d_31/b)})erfc(\frac{y\sqrt{1/b}}{2\sqrt{t}}+\sqrt{\frac{(a/b)t}{1/b}-d_3t}\right.$$
$$\left.+exp(-y\sqrt{(a/b-d_31/b)})erfc(\frac{y\sqrt{1/b}}{2\sqrt{t}}-\sqrt{\frac{(a/b)t}{1/b}-d_3t}\right),$$
$$f_{15}(y,t)=\frac{exp(-b_3t)}{2}\left(exp(y\sqrt{R-b_3Pr})erfc\left(\frac{y\sqrt{Pr}}{2\sqrt{t}}+\sqrt{\frac{Rt}{Pr}}\right)\right.$$

$-exp(-y\sqrt{R-b_3Pr})erfc\left(\frac{y\sqrt{Pr}}{2\sqrt{t}}-\sqrt{\frac{Rt}{Pr}}\right)\Big)$,

$f_{16}(y,t)=\left(\frac{exp(-c_3t)}{2}\right)\Big(exp(y\sqrt{(K_2-c_3)Sc})erfc(\frac{y\sqrt{Sc}}{2\sqrt{t}}+\sqrt{(K_2-c_3)t}$

$+exp(-y\sqrt{(K_2-c_3)Sc})erfc(\frac{y\sqrt{Sc}}{2\sqrt{t}}-\sqrt{(K_2-c_3)t}\Big)$,

$f_{17}(y,t)=\frac{exp(-d_3t)}{2}\Big(exp(y\sqrt{R-d_3Pr})erfc\left(\frac{y\sqrt{Pr}}{2\sqrt{t}}+\sqrt{\frac{Rt}{Pr}}\right)$

$-exp(-y\sqrt{R-d_3Pr})erfc\left(\frac{y\sqrt{Pr}}{2\sqrt{t}}-\sqrt{\frac{Rt}{Pr}}\right)\Big)$.

References

[1] Nalini Sethy, Debashis Mohanty, Ganeswar Mahanta, Sachin Shaw. Numerical analysis on thermal control and irreversibility for 3D Casson hybrid nanofluid flow within two permeable stretching surfaces with interfacial nanolayer thickness and slip velocities. Numer. Heat Transf B. 2023:1-23.

[2] Mohanty D, Mahanta G, Ali J. Chamkha, Shaw S. Numerical analysis of interfacial nanolayer thickness on Darcy-Forchheimer Casson hybrid nanofluid flow over a moving needle with Cattaneo-Christov dual flux. Numer. Heat Transf A. 2023: 1-25.

[3] Debashis Mohanty, Ganeswar Mahanta, Sachin Shaw. Analysis of irreversibility for 3-D MHD convective Darcy-Forchheimer Casson hybrid nanofluid flow due to a rotating disk with Cattaneo-Christov heat flux, Joule heating, and nonlinear thermal radiation. Numer. Heat Transf B. 2023; 84(2):115-142.

[4] Ali B, Liu S, Jubair S, Khalifa HAEW, Abd El-Rahman M. Exploring the impact of Hall and ion slip effects on mixed convective flow of Casson fluid Model: A stochastic investigation through non-Fourier double diffusion theories using ANNs techniques. Therm. Sci. Eng. Prog. 2023;46:102237.

[5] Ali B, Jubair S, Aluraikan A, Abd El-Rahman M, Eldin SM, Khalifa HAEW. Numerical investigation of heat source induced thermal slip effect on trihybrid nanofluid flow over a stretching surface. Results Eng. 2023;20;101536.

[6] Oyelakin IS, Sithole Mthethwa H, Kameswaran Peri K, Shaw S, Sibanda P. Entropy generation optimisation for unsteady stagnation Casson nanofluid flow over a stretching sheet with binary chemical reaction and Arrhenius activation energy using the bivariate spectral quasi-linearisation method. Int. J. Ambient Energy. 2022;43(1): 6489-6501.

[7] Mohanty D, Mahanta G, Shaw S, Sibanda P. Thermal and irreversibility analysis on Cattaneo-Christov heat flux-based unsteady hybrid nanofluid flow over a spinning sphere with interfacial nanolayer mechanism. J. Therm. Anal. Calorim. 2023; 148: 12269?12284.

[8] Naresh Kumar N, Sastry D.R.V.S.R.K, Sachin Shaw. Irreversibility analysis of an unsteady micropolar CNT-blood nanofluid flow through a squeezing channel with activation energy-Application in drug delivery. Comput. Methods Programs Biomed. 2022;226: 107156.

[9] Ali B, Duraihem FZ, Jubair S, Alqahtani H, Yagoob B. Analysis of interparticle spacing and nanoparticle radius on the radiative alumina based nanofluid flow subject to irregular heat source/sink over a spinning disk. Mater. Today Commun. 2023;36;106729.

[10] Elattar S, Helmi MM, Elkotb MA, El-Shorbagy MA, Abdelrahman A, Bilal M, Ali A. Computational assessment of hybrid nanofluid flow with the influence of hall current and chemical reaction over a slender stretching surface. Alex. Eng. J. 2022; 61(12); 10319-10331.

[11] Lund LA, Yashkun U, Shah NA. Multiple solutions of unsteady Darcy?Forchheimer porous medium flow of Cu?Al2O3/water based hybrid nanofluid with joule heating and viscous dissipation effect. J. Therm. Anal. Calorim. 2024; 1-13.

[12] Prakash R, Khan U, Gamaoun F, Sarada K, Nagaraja KV, Gill HS, Hassan AM. Thermal convection in rotating ferromagnetic liquid with thermorheological and magnetorheological effects. Case Stud. Therm. Eng. 2024;54, 104035.

[13] Madhukesh JK, Nagaraja KV, Gamaoun F, Prasannakumara BC. Impacts of nanoparticle aggregation and thermophoretic particle deposition on the flow of nanofluid over Riga wedge: a mathematical analysis. J. Therm. Anal. Calorim. 2023;148(24);14135-14144.

[14] Ali B, Mishra NK, Rafique K, Jubair S, Mahmood Z, Eldin SM. Mixed convective flow of hybrid nanofluid over a heated stretching disk with zero-mass flux using the modified Buongiorno model. Alex. Eng. J. 2023;72:83-96.

[15] Muller U, Buhler L, Magnetofluiddynamics in channels and containers. Springer. Germany (2001).

[16] Sivaraj R, Kumar B.R. Unsteady MHD dusty viscoelastic fluid Couette flow in an irregular channel with varying mass diffusion. Int. J. Heat Mass Transf. 2012;55(11-12):3076-3089.

[17] Ho J. Characteristic study of MHD pump with channel in rectangular ducts. J Mar Sci Technol. 2007;15:315-321.

[18] Homsy A, Linder V, Lucklum F, NF.de Rooij. Magnetohydrodynamic pumping in nuclear magnetic resonance environments. Sens. Actuators B: Chem. 2007;123:636-646.

[19] West J, Karamata B, Lillis B, Gleeson JP, Alderman, JK.Collins J, Lane W, Mathewson M, Berney H. Application of magnetohydrodynamic actuation to continuous flow chemistry. Lab on a Chip. 2002;2:224-230.

[20] Moffatt H.K. Electromagnetic Stirring. Phys. Fluids A. 1991;3:1336-1343.

[21] Zhao LZ, Ye HL, Peng AW, Zhang QH, Xia Q, Liu BL, Li J., Wang F, Li R. MHD wave energy underwater recharging platforms for AUVs. In Proceedings of the 26^th International Ocean and Polar Engineering Conference. 26 June-1 July 2016; 480-483.

[22] Niu XD, Yamaguchi H, Ye XJ, Iwamoto Y. Characteristics of a MHD power generator using a low-melting-point gallium alloy. Electr. Eng. 2012; 96: 37-43.

[23] Akbar NS, Tripathi D, Anwar Bég, Khan ZH. MHD dissipative flow and heat transfer of Casson fluids due to metachronal wave propulsion of beating cilia with thermal and velocity slip effects under an oblique magnetic field. Acta Astronaut. 2016;128:1-12.

[24] Prakash J, Siva E.P, Tripathi D, Kuharat S, Anwar Bég. Peristaltic pumping of magnetic nanofluids with thermal radiation and temperature-dependent viscosity effects: modelling a solar magneto-biomimetic nanopump. Renewable Energy.2019;133:1308-1326.

[25] Cramer KC, Pai SI. Magnetofluid Dynamics for Engineers and Applied Physicists. MacGraw-Hill. New York, USA 1973.

[26] Seddeek M. Effects of hall and ion-slip currents on magneto-micropolar fluid and heat transfer over a non-isothermal stretching sheet with suction and blowing. Proc. R. Soc. A: Math. Phys. Eng. 2016;457:3039-3050.

[27] Anwar Bég, Ferdows Enamu M, Karim M, Maruf Hasan M, Tasveer Beg A, Shamshuddin MD, Kadir B. Computation of non-isothermal thermo-convective micropolar fluid dynamics in a Hall MHD generator system with non-linear distending wall, Int J Appl Comput Math. 2020;6:1-44.

[28] Bhatti MM, Khalique CM, Tasveer Bég, Anwar Bég, Ali Kadir. Numerical study of slip and radiative effects on magnetic Fe_3O_4-water-based nanofluid flow from a nonlinear stretching sheet in porous media with Soret and Dufour diffusion. Mod. Phys. Lett. B. 2020;33: 2050026.

[29] Nasir S, Sirisubtawee S, Juntharee P, Berrouk AS, Mukhtar S, Gul T. Heat transport study of ternary hybrid nanofluid flow under magnetic dipole together with nonlinear thermal radiation. Appl. Nanosci. (2022);12(9):2777-2788.

[30] Nasir S, Berrouk A S. Comparative study of computational frameworks for magnetite and carbon nanotube-based nanofluids in enclosure. J. Therm. Anal.

Calorim. 2024;1-21.

[31] Nasir S, Berrouk A, Khan Z. Efficiency assessment of thermal radiation utilizing flow of advanced nanocomposites on riga plate. Appl. Therm. Eng. 2024;242:122531.

[32] Nasir S, Berrouk AS. Numerical and intelligent neuro-computational modelling with Fourier?s energy and Fick?s mass flux theory of 3D fluid flow through a stretchable surface. Eng. Appl. Comput. Fluid Mech. 2023;17(1):2270675.

[33] Gomathy G. Rushi Kumar B. Impacts of nanoparticle shapes on Ag?water nanofuid thin flm fow through a porous medium with thermal radiation and ohmic heating. J. Therm. Anal. Calorim, (2023).

[34] Postelnicu A. Influence of a magnetic field on heat and mass transfer by natural convection from vertical surfaces in porous media considering soret and dufour effects. Int. J. Heat Mass Transf. 2004;47:1467-1472.

[35] Makinde OD. On MHD mixed convection with soret and dufour effects past a vertical plate embedded in a porous medium. Lat. Am. Appl. Res. 2011; 41:63-68.

[36] Nasir S. Berrouk AS, Gul T, Ali A. Develop the artificial neural network approach to predict thermal transport analysis of nanofluid inside a porous enclosure. Sci. Rep. 2023;13(1):21039.

[37] Gul T, Nasir S, Berrouk AS, Raizah Z, Alghamdi W, Ali I, Bariq A. Simulation of the water-based hybrid nanofluids flow through a porous cavity for the applications of the heat transfer. Sci. Rep. (2023);13(1);7009.

[38] Saeed A, Kumam P, Nasir S, Gul T, Kumam W. Non-linear convective flow of the thin film nanofluid over an inclined stretching surface. Sci. Rep. 2021;11(1);18410.

[39] Nasir S, Alghamdi W, Gul T, Ali I, Sirisubtawee S, Aamir A. Comparative analysis of the hydrothermal features of TiO2 water and ethylene glycol-based nanofluid transportation over a radially stretchable disk. Numer. Heat Transf. B: Fundam. 2023;83(5): 276-291.

[40] Siva Reddy Sheri, Anwar Bég, Modugula P, Kadir A. Computation of transient radiative reactive thermo-solutal magneto-hydrodynamic convection in inclined MHD Hall generator flow with dissipation and cross diffusion. Comput. Therm. Sci. 2019; 11: 541-563.

[41] Anwar Bég, Tasveer A. Bég, Karim I, Khan MS, Alam MM, Ferdows M, Shamshuddin M. Numerical study of magneto-convective heat and mass transfer from inclined surface with Soret diffusion and heat generation effects. Chinese J. Physics. 2019;60:167-179.

[42] Koester JK, Perkins RA. Discharge and corrosion characteristics of slagging metal electrodes for MHD power generators. J. Mater. Energy Sys. 1979;1:41-54.

[43] Abdallah IA. Analytic solution of heat and mass transfer over a permeable stretching plate affected by chemical reaction, internal heating, dufour-soret effect and Hall effect. Therm. Sci. 2009; 13: 183-197.

[44] Makinde OD, Olanrewaju PO. Unsteady mixed convection with Soret and Dufour effects past a porous plate moving through a binary mixture of chemically reacting fluid. Chem. Eng. Commun. 2011; 198:920-938.

[45] Kandasamy R, Periasamy K, Prabhu KS. Chemical reaction, heat and mass transfer on MHD flow over a vertical stretching surface with heat source and thermal stratification effects. Int. J. Heat Mass Transf. 2005;48:4557-4561.

[46] Seth G, Kumbhakar B, Sharma R. Unsteady mhd free convection flow with hall effect of a radiating and heatabsorbing fluid past a moving vertical plate with variable ramped temperature. J. Egypt. Math. Soc. 2016;24: 471-478.

[47] Seth G, Sarkar S, Hussain SM. Effects of hall current and rotation on hydromagnetic natural convection flow with heat and mass transfer of a heat absorbing fluid past an impulsively moving vertical plate with ramped temperature. J. Appl. Fluid Mech. 2014;8:159-171.

[48] Kataria H, Patel H. Heat and mass transfer effects on unsteady free convective mhd flow of a micro polar fluid between two vertical walls. Math Today. 2018;34:42-63.

[49] Mantripragada S, Wang X, Gordaninejad F, Hu B, Fuchs A. Rheological properties of novel magnetorheological fluids. Int. J. Mod. Phys. B. 2007;21:4849-4857.

[50] Kataria HR, Patel HR. Effects of chemical reaction and heat generation/absorption on magnetohydrodynamic (MHD) Casson fluid flow over an exponentially accelerated vertical plate embedded in porous medium with ramped wall temperature and ramped surface concentration. Propuls. Power Res. 2019;8:35-46.

[51] Patel HR. Effects of heat generation, thermal radiation, and hall current on MHD Casson fluid flow past an oscillating plate in porous medium. Multiph. Sci. Technol. 2019;31.

[52] Sulochana C, Payad SS, Sandeep N. Non-uniform heat source or sink effect on the flow of 3D Casson fluid in the presence of Soret and thermal radiation. Int. J. Eng. Res. 2018;20:112-129.

[53] Anwar Bég, Tasveer Bég, Munjam SR, Jangili S. Homotopy and Adomian semi-numerical solutions for oscillatory flow of partially ionized dielectric hydrogen gas

in a rotating MHD energy generator duct. Int. J. Hydrog. Energy. 2021;46:17677-17696.

[54] Matsumoto M, Murakami T, Okuno Y. Numerical study on the feasibility of a pulsed heat source high temperature inert gas MHD electrical power generation. Trans. Jpn. Soc. Aeronaut. Space Sci. 2008;51:164-169.

[55] Hamad M, Pop I. Unsteady MHD free convection flow past a vertical permeable flat plate in a rotating frame of reference with constant heat source in a nanofluid. Heat Mass Transf. 2011;47:1517-1524.

[56] Ram P. Effects of Hall and ion-slip currents on free convective heat generating flow in a rotating fluid. Int. J. Energy Res. 1995;19:371-376.

[57] Krishna MV, Chamkha AJ. Hall and ion slip effects on unsteady MHD convective rotating flow of nanofluids application in biomedical engineering. J. Egypt. Math. Soc. 2020;28:1-15.

[58] Krishna MV, Chamkha AJ. Hall and ion slip effects on MHD rotating flow of elastico-viscous fluid through porous medium. Int. J. Heat Mass Transf. 2020;113:104494.

[59] Nandkeolyar R, Seth G, Makinde OD. Unsteady hydromagnetic natural convection flow of a dusty fluid past an impulsively moving vertical plate with ramped temperature in the presence of thermal radiation. J. Appl. Mech. 2013;80.

[60] Ghosh SK, Anwar Bég, Zueco J, Prasad. Transient hydromagnetic flow in a rotating channel permeated by an inclined magnetic field with magnetic induction and Maxwell displacement current effects. J. Applied Mathematics and Physics. 2010;61:147-169.

Nomenclature

$\overline{V}$	velocity vector (m/s)
$\overline{E}$	electric field intensity vector (V/m)
$\overline{B}$	applied magnetic field vector $(Tesla)$
J	electric density (V/m)
m	hall current (m^3/C)
t^*	dimensional time (s)
q	heat flux (Wm^{-2})
τ	shear stress (Nm^{-2})
Ω	angular velocity (rad/s)
σ	electrical conductivity of non-Newtonian fluid (S/m)
n_e	number of density electrons (eA^{-3})
U,W	dimensional velocity components along X, Z directions (m/s)
g	gravitational acceleration (m/s^2)
Rd	radiation parameter (-)
Nu	Nusselt number (-)
Sh	Sherwood number (-)
γ	Casson fluid parameter (-)
B_0	magnetic field $(kgs^{-2}A^{-1})$
Pr	Prandtl number (-)
ρ	density (kgm^{-3})
Sc	Schmidt number (-)
$erfc$	Complementary error function (-)
erf	Error function (-)
K_1	porous medium permeability (-)
κ	thermal conductivity $(Wm^{-1}K^{-1})$
σ^*	Stefan-Boltzmann radiation constant $(Wm^{-2}s^{-4})$
Gm	solutal Grashof number (-)
K_2	chemical reaction parameter (-)
K	rotational parameter (-)
T	fluid Temperature (K)
u, w	velocity components(dimensionless)(m/s)
Gr	thermal Grashof number (-)
Q	heat source/sink (-)
Sr	Soret effect parameter (-)
M	magnetic parameter (-)
μ_β	dynamic viscosity of fluid (kg/ms^3)
π_e	critical value of product (-)
py	yield stress of fluid (-)
$H(\cdot)$	Heaviside unit step function (-)